




Mesoscale Simulation on the Effect of Elevated Temperature on Dynamic Compressive Behavior of Steel Fiber Reinforced Concrete

Liu Jin, Huimin Hao, Renbo Zhang * and Xiuli Du*, Key Laboratory of Urban Security and Disaster Engineering of Ministry of Education, Beijing University of Technology, Beijing 100124, China

Received: 28 August 2019/**Accepted:** 16 January 2020

Abstract. Steel fiber reinforced concrete (SFRC) is an appropriate material for protective structure and may undergo fire, impact and the coupled effects of them. To investigate the dynamic failure behavior of SFRC after elevated temperature, a mesoscale simulation method was established. In the approach, the SFRC was regarded as a four-phase composite material consisting of aggregate particles, mortar matrix and the interfacial transition zones between them as well as fibers. Each phase has its own independent thermal and mechanical properties. During the simulations, a sequentially coupled thermal-stress procedure was employed. In detail, thermal conduction within SFRC specimens was conducted firstly. Then, taking the results of damage and temperature field as the initial state, the dynamic failure behavior of SFRC under uniaxial compression was modelled. Comparison between simulation results and experimental observations reveals the rationality and accuracy of the simulation method. Based on the calibrated simulation approach, the mechanical performances of SFRC under various temperature and strain rates were simulated. Both the temperature degradation and strain rate enhancement effects on the apparent property of SFRC were studied. The results indicate that steel fiber can effectively improve the dynamic mechanical properties of concrete after high temperature and more adequately prevent crack evolution under high strain rate. The fiber enhancement effect on strength is weakened with the increase of strain rate, while that is more significant with the increase of temperature.

Keywords: Steel fiber reinforced concrete, Elevated temperature, Dynamic compression, Strain rate effect, Meso-scale

1. Introduction

Engineering structures, especially protective structures may be subjected to extreme loadings such as fire, impact and their combined effects, except for regular loadings during their service life [1]. Plain concrete is one of the most com-

* Correspondence should be addressed to: Renbo Zhang, E-mail: zhangrenbo99@126.com; Xiuli Du, E-mail: duxiuli2015@163.com



monly used construction materials, whose mechanical properties will be changed in different degrees under dynamic loads (e.g. explosion and impact) and high temperature (fire). To better understand the behavior of structures suffering extreme events, the properties of construction materials in those cases should be explored firstly. Thence, many scholars studied the mechanical properties of concrete materials under high temperature and high strain rate. Furthermore, some researchers explored ameliorative methods to make up the defects of concrete materials. Among these, addition of discontinuous fibers (steel fiber, polypropylene fiber etc.) is the most widely used for concrete because of the satisfactory toughness and bridging effect of the fibers.

1.1. Plain Concrete

Concrete has been sufficiently studied to predict its behavior at various loading scenarios by experiment and simulation methods. Huo et al. [2] carried out dynamic compressive tests for concrete specimens after exposure to elevated temperatures by using Split Hopkinson Pressure Bar apparatus. Chen et al. [3] reported an experimental study of the combined effects of high temperature and high strain rate on normal concrete material. The dynamic residual mechanical properties of concrete after exposure to high temperature were investigated by Park and Yim [4]. It is proved that property of plain concrete is depended on both temperature and strain rate when undergoing fire and impact. In general, the strain rate effect (i.e., strength of concrete is increased with an increasing strain rate) can be attributed to thermal activation, macro-viscosity and inertial mechanism [5–9]. Moreover, strain rate effect is influenced by various uncertain factors, for example, composition, water-to-cement ratio, curing method and time, aggregate type, specimen size and experimental techniques [6, 8]. While exposed to fire, concrete is degraded significantly by elevated temperatures and loses much of its load carrying capacity. To evaluate the temperature effect quantitatively, reduction factors and design curves are adopted in codes [10].

1.2. Steel Fiber Reinforced Concrete

In recent years, many scholars have paid attention to the research of fiber reinforced concrete to reduce the loss caused by extreme load, including polypropylene fiber, steel fiber and hybrid fiber etc. Steel fiber reinforced concrete (SFRC), combining a cementitious matrix and a discontinuous reinforcement, consisting of steel fibers randomly distributed in the matrix, has good toughness and high tensile strength and can improve the shortage of traditional plain concrete, such as low tensile strength and brittleness [11]. Therefore, SFRC is an appropriate material for protective structures. During the last several decades, a large number of investigations have been conducted to study the property of SFRC [12–16]. Dügenci et al. [17] investigated the results of the effect of high temperature on SFRC. An experimental study on uniaxial mechanical properties of SFRC subjected to high strain-rate compressive loading was presented by Sun et al. [18]. Yoo and Banthia [19] examined rate dependent fiber pullout behavior, dynamic compressive behavior, impact tensile and flexural behaviors of ultra-high-perfor-

mance fiber reinforced concrete at material level. These results reflected that although different from plain concrete, SFRC is still strain rate- and temperature-dependent.

Nevertheless, the effect of strain rate or temperature is studied separately in most of the available literatures while their combined effect is relatively less concerned due to limit of experimental techniques. Caverzan et al. [20], Xiao et al. [21], Zhai et al. [22], and Yao et al. [23] conducted a series of tests to study the behavior of mortar, normal weight concrete and high strength concrete under both high strain rate and elevated temperature. Considering the heterogeneity of concrete inner structure, Jin et al. [24] conducted a mesoscopic simulation on dynamic compressive behavior of plain concrete at/after elevated temperature. It is found that influenced by high temperatures, materials become more brittle and show different strain rate effect compared with that in room temperature. However, the available efforts are far from quantitatively determining the combined effects of strain rate and elevated temperature. When it comes to SFRC, there is almost no research on its properties subjected to both fire and impact.

1.3. The Present Study

The focus of the present work is on the combined effects of strain rate and temperature on the global mechanical properties of SFRC. Considering that the macroscopic property of material is closely related to its inner structure, a mesoscopic numerical model to simulate its behavior under various strain rates and temperatures was established. From the viewpoint of meso-scale, the SFRC was regarded as a four-phase composite material consisting of aggregate particles, mortar matrix and the interfacial transition zones (ITZs) between the above mentioned two phases, as well as the steel fibers. Each phase has its own independent thermal and mechanical properties. During the simulations, thermal conduction within SFRC specimens was conducted firstly. Then, regarding the results of damage and temperature field as the initial state, the dynamic compressive failure behavior of SFRC under mechanical loadings was simulated sequentially. Based on the verified simulation procedure, both the temperature degradation and strain rate enhancement effects on the apparent mechanical properties of SFRC were analyzed and discussed.

2. Meso-Scale Simulation Method of SFRC

In this section, the meso-scale numerical simulation method for SFRC will be introduced. To establish the FE model and solve the FE equations, the commercial software ABAQUS [25] was employed.

2.1. Simulation Procedures

To study the effect of elevated temperature on dynamic mechanical behavior of SFRC, it was assumed that thermal and mechanical loading processes are one-way coupled and a sequentially coupled procedure was adopted. In detail, the

stress solution is influenced by temperature field while no inverse effect exists. Accordingly, the simulation process can be divided into two steps and this treatment is similar to that in Jin et al.'s work [24]. Firstly, simulation of thermal conduction within SFRC was carried out to obtain the thermal damage and the temperature field experienced by SFRC specimens. Secondly, by taking the obtained damage distribution and temperature field results (i.e., the output results, which determines the residual mechanical properties of concrete) from the first step as an initial state, the dynamic failure behavior of SFRC was conducted with temperature-related parameters.

2.2. Mesoscopic Geometry Model

To analyze the dynamic mechanical performance of SFRC after elevated temperature, taking the fact that macroscopic apparent property is closely related to the inner structure of materials into account, a meso-scale geometry model which can better describe the material structure was established for SFRC. From the viewpoint of meso-scale, SFRC can be considered as a four-phase composite consisting of coarse aggregate, mortar matrix and ITZs between them as well as randomly distributed steel fibers. The coarse aggregate particles were supposed as circular here for simplicity, which is similar to the relevant literature [26]. These particles were involved in mortar matrix with a “take and place” method based on Monto Carlo theory [24]. This method can guarantee that aggregate particles were distributed randomly and apart from each other while no overlap between them. According to the available literatures [27, 28] and our previous study [29, 30], the distribution of coarse aggregate mainly affects the local behavior while has a quite small influence on the global performance of concrete. Thence, only one random distribution pattern was considered in the following simulations.

The ITZs are regarded as a band area along the circumference of aggregate, which are endowed with independent material (i.e. weakened mortar) properties. What needs illustration is that the real thickness (about 10–100 μm) of ITZs is difficult to be simulated accurately due to the limitation of the calculation amount and mesh size [31, 32]. Thence, the thickness of ITZs was set to 1 mm according to the work of Šavija et al. [33] and Du et al. [34]. As for steel fibers, their positions and orientations were also determined randomly and the operation process was similar to that for aggregate particles. In order to be close to the reality, fibers were placed into mortar and ITZs without invasion into aggregate regions. Therefore, a random aggregate model was obtained.

The meso-scale numerical simulation model of steel fiber reinforced concrete (SFRC) and plain concrete (PC) established with the abovementioned method are presented in Fig. 1, respectively. Dimension of the concrete specimen was 150 mm \times 150 mm and the length of steel fibers was selected as 30 mm. In Fig. 1, the green circle areas represent aggregate particles, whose content is about 47% by volume, containing 6 middle stone particles (diameter $d = 30$ mm) and 56 small stone particles (diameter $d = 12$ mm). The red band region around the aggregate particles represent the interface transition zones (ITZs) and the gray zones mean the mortar phase, which are the same as those in [24]. Besides, the

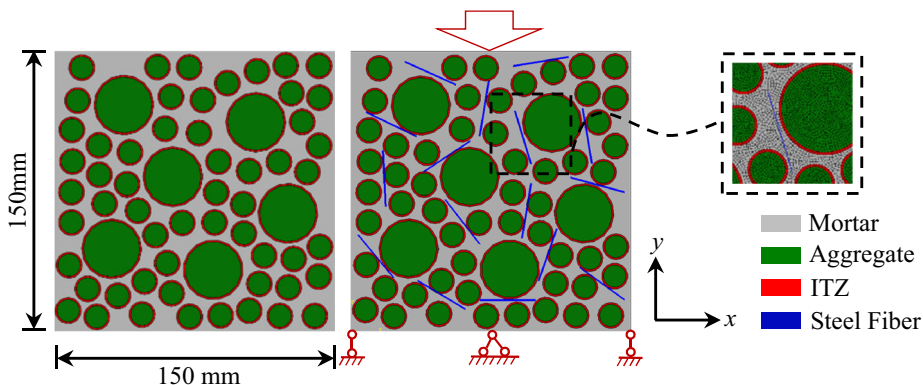


Figure 1. Meso-scopic models of heterogeneous concrete specimens.

blue areas mean steel fibers which were embedded in mortar and ITZs and the volume fraction of steel fibers of 1% was utilized.

Similar to the work of Xu et al. [35], the positions and orientations of steel fibers are placed randomly. As it is well known, there exists complex bond-slip actions between fiber and concrete matrix, especially for SFRC subjected to combined effects of high strain rate and high temperature. Some studies [16, 36, 37] have simulated the interaction using the simplified one-dimensional contact algorithm under different loadings. However, the impeccable interaction relationship between fiber and concrete matrix cannot be given due to the lack of relevant studies on the dynamic mechanical properties of the fiber/matrix interfaces at/after elevated temperature. In view of this, an ideal bond between fibers and mortar matrix was assumed preliminarily in the present study. It must be illustrated that the treatment is therefore a rough approximation.

It should be noted that for the purpose of saving model and computation cost, the size and number of aggregate and steel fiber were modified equivalently while identical volume fractions to those in reality were set. To discretize the computational area, a four-node quadrilateral iso-parametric element was adopted for concrete and a two-node beam element was used for fibers. Element types of heat transfer and plain strain were employed for analysis of thermal conduction and dynamic loading processes, respectively. The corresponding mesh size was set as 1 mm [24].

2.3. Constitutive Relationships and Parameters

2.3.1. *Thermal Conduction* Assuming that thermal conduction within SFRC can be described by Fourier law [24, 30], the classical heat conduction equations can be described as [38]:

$$k \frac{\partial^2 T}{\partial x_i^2} = \rho c \frac{\partial T}{\partial t} \tag{1}$$

where k is thermal conductivity; ρ is the mass density; c is the specific heat capacity.

The thermal conductivity, specific heat capacity and mass density become the essential parameters for the computation of temperature field. Similar with that in [24, 30], these three parameters for meso-components of concrete were considered as temperature-related. Referring to the work of Jin et al. [30] and Zoth and Hänel [39], the temperature dependency of thermal conductivity can be calculated as:

$$k_T/k_0 = 1.026 - 0.013\left(\frac{T}{100}\right) + 0.0043\left(\frac{T}{100}\right)^2 \quad (2)$$

$$k_{aT} = \frac{770}{0.84(350 + T)} + 0.7 \quad (3)$$

In addition, based on the summary of Černý et al. [40] as well as Vosteen and Schellschmidt [41], the temperature-dependent formula for specific heat capacity can be expressed as:

$$c_T = 790 + 0.9T \quad (4)$$

$$c_{aT} = (1 + T)^{0.075} \quad (5)$$

in which k_T and c_T are thermal conductivity, specific heat capacity of mortar and ITZs, respectively; k_{aT} and c_{aT} represent thermal conductivity and specific heat capacity of aggregate, respectively; and k_0 is thermal conductivity of mortar and ITZs at room temperature. Referring to the result of Grassl and Pearce [42], the temperature dependency of thermal expansion coefficient of the meso-phase can be described as:

$$\alpha_T(T) = \alpha_{T1} + \alpha_{T2}(T - T_a) + \alpha_{T3}(T - T_a)^2 \quad (6)$$

in which α_T is the thermal expansion coefficient, T_a is reference temperature (20°C), α_{T1} , α_{T2} and α_{T3} are the model parameters, which are listed in Table 1. CEB code [43] has provided the ratio between mass density (ρ_T) at high temperatures and that (ρ_0) at room temperature for concrete, it can be described as:

$$\rho_T/\rho_0 = \begin{cases} 1 - \frac{0.02(T-115)}{85} & 115^\circ\text{C} < T \leq 200^\circ\text{C} \\ 0.98 - \frac{0.03(T-200)}{200} & 200^\circ\text{C} < T \leq 400^\circ\text{C} \\ 0.95 - \frac{0.07(T-400)}{800} & 400^\circ\text{C} < T \leq 1200^\circ\text{C} \end{cases} \quad (7)$$

Table 1
Thermal Parameters for Materials at Room Temperature (20°C)

Materials	Thermal conductivity, k [W/(m K)]	Mass density, ρ [kg/m ³]	Special heat capacity, c [J/(kg K)]	Thermal expansion coefficient (°C ⁻¹)		
				α_{T1}	α_{T2}	α_{T3}
Aggregate	3.15 ^a	2750	798 ^b	1.5×10^{-6}	7.0×10^{-8}	0
ITZ	0.7	2450	906	1.5×10^{-6}	0	-6.0×10^{-11}
Mortar	1.9 ^a	2250	813 ^c	1.5×10^{-6}	0	-6.0×10^{-11}
Steel	45	7850	600	1.4×10^{-5}	0	0

The adopted data with superscript “a” are taken from [45], those with “b” are quoted from [41], and the data with “c” are taken from [21]. All the data for steel are from [44]; all data of thermal expansion coefficient for meso-components of concrete are adopted from [42]

It is worth noting that the thermal parameters (i.e., thermal conductivity, mass density and specific heat capacity) for steel were treated as constant at elevated temperatures according to Chinese code [44]. Since temperature-dependent parameters of concrete were obtained based on that at ambient temperature, all the involved thermal parameters at room temperature are listed in Table 1. Herein, the data with superscripts “a”, “b” and “c” were taken from the work of Ref. [45], Ref. [41] and Ref. [21], respectively.

2.3.2. *Simulations on Mechanical Behavior* Similar with Jin et al. [24], the mechanical behavior of aggregate was described by ideal elastoplastic constitutive model after elevated temperature. Moreover, similar with those in references [46–48], the damaged plasticity constitutive model proposed by Lubliner et al. [49] and modified by Lee and Fenves [50] which can well describe the failure behavior of concrete under complex stress state and dynamic loadings was utilized to describe the property of mortar matrix and the ITZs. The constitutive model assumes that the uniaxial tensile and compressive responses of concrete are characterized by damaged plasticity, and the failure forms of concrete material is mainly divided into tensile crack and compression failure. Herein, the stress–strain relationships under tension and compression can be described respectively:

$$\sigma_t = (1 - d_t)D_0^{el} : (\boldsymbol{\varepsilon}_t - \boldsymbol{\varepsilon}_t^{pl}) \tag{8}$$

$$\sigma_c = (1 - d_c)D_0^{el} : (\boldsymbol{\varepsilon}_c - \boldsymbol{\varepsilon}_c^{pl}) \tag{9}$$

where D_0^{el} presents the initial elasticity matrix; d_t and d_c mean the tensile and compressive damage variables, respectively; $\boldsymbol{\varepsilon}_t^{pl}$ and $\boldsymbol{\varepsilon}_c^{pl}$ present the plastic tensile and compressive strain tensors, respectively. Both the strain rate enhancement and temperature degradation effects were considered and the corresponding relationships are the same as those in the previous work [24].

The strain rate effect on concrete after exposure to fire are not commonly acknowledged, and it is found the dynamic strain rate effect after high temperature has little change according to the result of Zhai et al. [51]. Herein, it was provisionally assumed that strain rate effect of concrete after elevated temperature is similar to that at room temperature. Accordingly, the dynamic increase factor DIF (i.e. the ratio between dynamic strength and quasi-static strength) can be used to characterize the amplification effect of strength. The CEB code [43] has given the equations for dynamic compressive and tensile strength as well as Young's modulus of concrete, and they can be expressed as:

$$\text{CDIF} = f_{c,\text{imp},k}/f_{\text{cm}} = \begin{cases} (\dot{\epsilon}_c/\dot{\epsilon}_{c0})^{0.014}, & \dot{\epsilon}_c \leq 30 \text{ s}^{-1} \\ 0.012(\dot{\epsilon}_c/\dot{\epsilon}_{c0})^{1/3}, & \dot{\epsilon}_c > 30 \text{ s}^{-1} \end{cases} \quad (10)$$

$$\text{TDIF} = f_{\text{ct},\text{imp},k}/f_{\text{ctm}} = \begin{cases} (\dot{\epsilon}_{\text{ct}}/\dot{\epsilon}_{\text{ct}0})^{0.018}, & \dot{\epsilon}_{\text{ct}} \leq 10 \text{ s}^{-1} \\ 0.0062(\dot{\epsilon}_{\text{ct}}/\dot{\epsilon}_{\text{ct}0})^{1/3}, & \dot{\epsilon}_{\text{ct}} > 10 \text{ s}^{-1} \end{cases} \quad (11)$$

$$E_{c,\text{imp}}/E_c = (\dot{\epsilon}_c/\dot{\epsilon}_{c0})^{0.026} \quad (12)$$

in which $E_{c,\text{imp}}$ and E_c are the dynamic and static elastic modulus, respectively; $f_{c,\text{imp},k}$, $f_{\text{ct},\text{imp},k}$ are the dynamic compressive and tensile strength of meso-components when the strain rate equals to $\dot{\epsilon}_c$ and $\dot{\epsilon}_{\text{ct}}$, respectively; f_{cm} is the quasi-static compressive strength when strain rate $\dot{\epsilon}_{c0} = 30 \times 10^{-6} \text{ s}^{-1}$; f_{ctm} is the quasi-static tensile strength when strain rate $\dot{\epsilon}_{\text{ct}0} = 1 \times 10^{-6} \text{ s}^{-1}$.

At present, the assumption was made that temperature degradation degree of mechanical performance for mortar matrix and ITZs is similar to those of concrete. According to the parameters specified in Eurocode 2 [10] for the compressive and tensile strengths of concrete at elevated temperatures, its degradation relationship with temperature can be fitted as Eqs. (13) and (14), respectively.

$$f_{cT}/f_c = 1.037 - 2 \times 10^{-3}T - 8 \times 10^{-7}T^2 \quad (13)$$

$$f_{iT}/f_i = 1 - (T - 100)/500 \quad (14)$$

The degradation relationship of elastic modulus about temperature recommended in [39] was employed.

$$E_T/E = 0.83 - 1.1 \times 10^{-3}T, \quad 60^\circ\text{C} \leq T < 700^\circ\text{C} \quad (15)$$

Since f_{iT}/f_i gets negative when the temperature exceeded 500°C , it is assumed to be a constant (the value equal to that under $T = 500^\circ\text{C}$) when $T \geq 500^\circ\text{C}$. Among them, the subscript T denotes the mechanical parameters after high temperature.

When it comes to aggregate, the strength and Young’s modulus at room temperature were taken from [52] while their temperature degradation relationships were obtained according to the experimental data in [53].

The temperature degradation curves for mechanical properties of the meso-scale components of concrete has been demonstrated in Fig. 2. In addition, the main mechanical parameters for meso-constituents at room temperature were tabulated in Table 2. Herein, the data with superscript “^” are taken from [52].

The steel fibers were considered as an ideal elastoplastic material. The temperature degradation of Young’s modulus (E_s) and yielding strength (f_y) of steel material was described by Eqs. (16) and (17), respectively, as per [44]. Meanwhile, the strain rate effect on yielding strength was considered as Eq. (18) according to CEB Bulletin [54].

$$E_{sT}/E_s = \begin{cases} \frac{7T-4780}{67-4760} & 20^\circ\text{C} \leq T < 600^\circ\text{C} \\ \frac{1000-T}{67-2800} & 600^\circ\text{C} \leq T < 1000^\circ\text{C} \end{cases} \quad (16)$$

$$f_{yT}/f_y = \begin{cases} 1.0 & 20^\circ\text{C} \leq T < 300^\circ\text{C} \\ 1.24 \times 10^{-8}T^3 - 2.096 \times 10^{-5}T^2 + 9.228 \times 10^{-3}T - 0.2168 & 300^\circ\text{C} \leq T < 800^\circ\text{C} \\ 0.5 - T/2000 & 800^\circ\text{C} \leq T < 1000^\circ\text{C} \end{cases} \quad (17)$$

$$f_{yd}/f_{ys} = 1.0 + (6.0/f_{ys})\ln(\dot{\epsilon}_s/\dot{\epsilon}_{s0}) \quad (18)$$

in which, f_{yd} and f_{ys} are the dynamic and static yielding strengths, in MPa; $\dot{\epsilon}_s$ and $\dot{\epsilon}_{s0}$ are the dynamic and quasi-static strain rates, respectively, $\dot{\epsilon}_{s0} = 50 \times 10^{-5} \text{ s}^{-1}$.

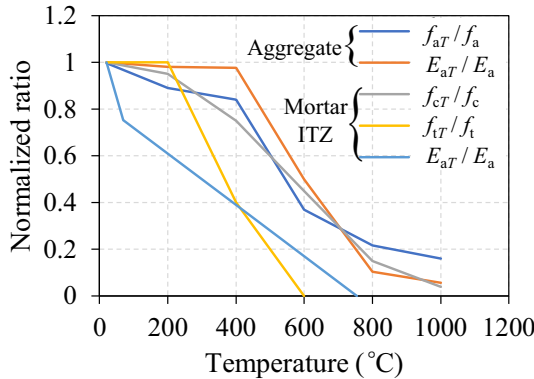


Figure 2. Ratio between mechanical properties of concrete after different temperature exposure to those in the case of room temperature.

Table 2
Mechanical Parameters for Materials at Room Temperature (20°C)

Material	Compressive strength, f_c [MPa]	Tensile strength, f_t [MPa]	Elastic modulus, E [GPa]	Poisson's ratio, ν
Aggregate	152 [^]	–	35 [^]	0.2
ITZ	32.5	3.25	30	0.2
Mortar	40	4	25	0.2
Steel	1100	1100	210	0.3

The adopted data with superscript “[^]” are taken from [52]

2.4. Boundary and Loading Conditions

2.4.1. Initial Temperature Field During the simulation of thermal conduction, initial temperature of SFRC specimen was set as ambient temperature. It was assumed that all the SFRC specimens were exposed to elevated temperature following the ISO 834 standard fire curve [55]. Then these SFRC specimens were heated up to the desired target temperature and exposed for 2 h or more to obtain an even temperature field.

2.4.2. Mechanical Loading After the simulation of heat conduction, the bottom side of specimen was restraint vertically while a vertical displacement with constant velocity v was applied on the top side, as illustrated in Fig. 1. The other sides were supposed as free. Accordingly, the apparent strain rate $\dot{\epsilon}$ undergone by specimen can be calculated as $\dot{\epsilon} = v/h$, in which, h is the height of specimen.

3. Simulation Results and Analysis

3.1. Verification of the Present Approach

Gao [56] investigated the mechanical properties of fiber reinforced concrete and plain concrete after exposure to elevated temperature using a microcomputer control electro hydraulic servo wire testing machine. In the experiment, the side length of SFRC specimens was 70 mm and the length of the steel fiber utilized was 30 mm, whose volume fraction can be calculated as 1%. The 28-day aged cubic concrete specimens were heated to target temperature with a heating rate of 10°C/min and maintained constant temperature for 3 h by a smart-box-type electric furnace. Then, the specimens were cooled down in air and tested after 7 days. To calibrate the meso-scale simulation method, all the parameters available in the experiment, including specimen size, fiber content and length as well as heating rate, were employed in the numerical model. The simulated stress–strain relationship of concrete specimens ($T = 20^\circ\text{C}$ and 800°C) was obtained and compared with the experimental data, as plotted in Fig. 3. In which, JF represents plain concrete, SF means SFRC. One can note that the numerical results are in good agreement with the experimental phenomenon. Therefore, the present method can be applied to study the high temperature compressive behavior of SFRC.

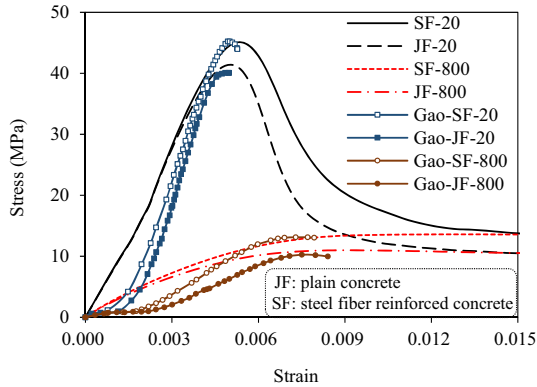


Figure 3. Comparison between the simulated stress–strain curves and Gao’s [50] experiment results.

3.2. Effect of Fiber Length

Figure 4 shows the comparison between failure patterns of the steel fiber reinforced concrete with different fiber length subjected to strain rate $\dot{\epsilon} = 1 \text{ s}^{-1}$ after different temperature exposure conditions. It can be observed that the number of cracks of the concrete specimens is strongly decreased with the addition of steel fiber, which can be explained by the good transverse bridging property of the steel fiber that prevents the development and extension of cracks inside the concrete materials. Moreover, the stress–strain relationship of SFRC with different steel fiber length was illustrated in Fig. 5. It is not hard to find that both ultimate strength and residual strength of SFRC increase with the growth of fiber length no matter at room temperature or after elevated temperatures. This phenomenon manifests that the steel fiber can effectively improve mechanical properties of plain concrete after elevated temperature, including both strength and toughness. Moreover, the enhancement becomes more significant with the increase of fiber length. Thence, in the following analysis, SFRC with fiber length of 30 mm will be taken as an example.

3.3. Results and Discussions

3.3.1. Damage Patterns of SFRC Figure 6 present the equivalent plastic strain of SFRC specimen and the von Mises stress of steel fiber after exposure to 800°C under the strain rate of 10 s^{-1} , respectively. It can be noticed that stress is concentrated on vertical fibers whose direction is similar to the loading and cracking direction. As loading goes on, the crack begins with the periphery of the fibers and extends gradually to ITZs and mortar matrix.

Figure 7 displays the damage results of SFRC subjected to elevated temperature under different strain rates. This is not hard to find that the crack modality is closely related to the strain rate and temperature. According to horizontal observation Fig. 7, under the same temperature, the fragmentation of concrete gets more serious with increasing nominal strain rate. The crack gradually widens as the

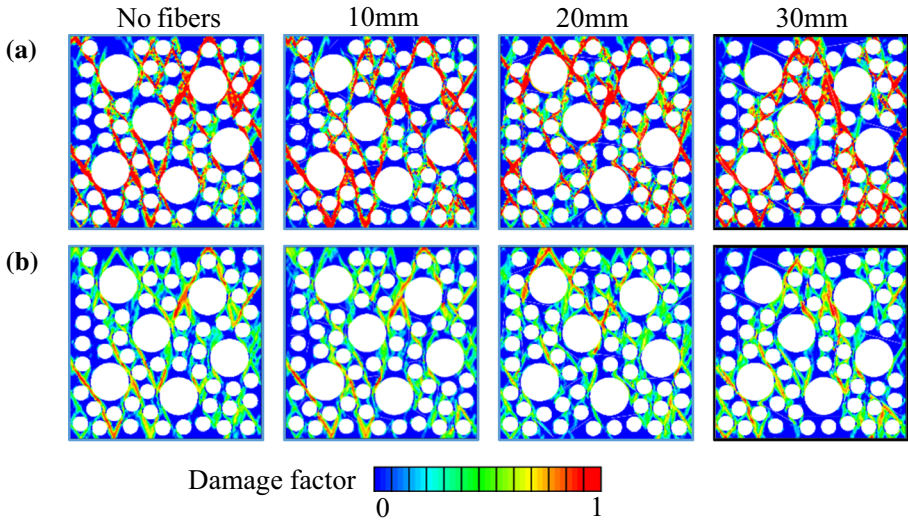


Figure 4. Comparison between the failure patterns of SFRC with different steel fiber length under strain rate $\dot{\epsilon} = 1 \text{ s}^{-1}$. a $T = 20^\circ\text{C}$; b $T = 800^\circ\text{C}$.

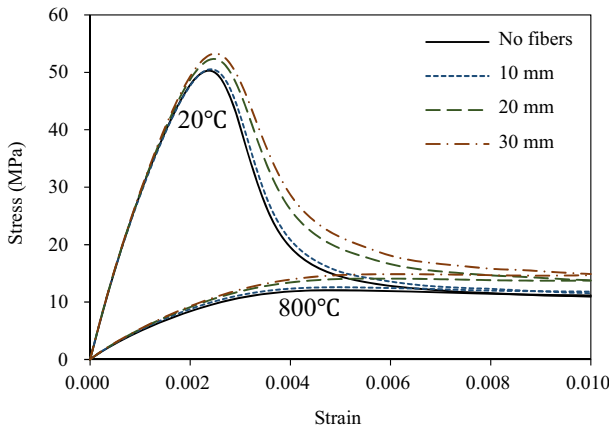


Figure 5. Stress-strain relationship of SFRC with different steel fiber length.

impact velocity increases, the failure patterns of SFRC specimen change from crack failure to crush mode. The phenomenon is consistent with that for plain concrete. While, according to vertical observation, under the same nominal strain rate, the dynamic destruction seems to be slowed down with increasing temperature. This is attributed to the fact that the concrete material is more and more incompact under high temperature with a decreasing strength and an increasing ductility. Moreover, the improvement effect of steel fibers on concrete materials

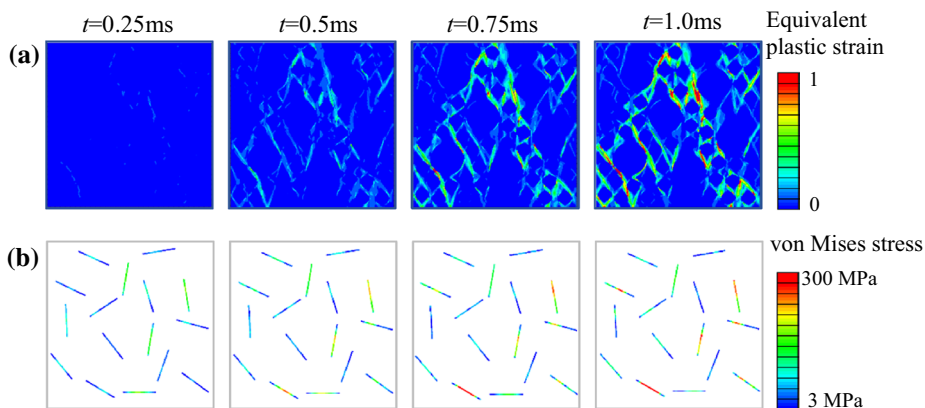


Figure 6. Damage process of the SFRC with the strain rate $\dot{\epsilon} = 10 \text{ s}^{-1}$ exposed to fire for 800°C .

after high temperature is more obvious. This may be interpreted by that on the one hand, the good thermal conduction performance of the randomly distributed steel fibers can make the temperature field within specimens more even, thus reducing the cracks caused by thermal gradient and improving the performance of SFRC [5]. On the other hand, the greater dilatancy of concrete at high temperature activates the steel fibers to play their role as confinement, thus enhancing the SFRC [57, 58].

3.3.2. Stress Distributions of Steel Fiber Figure 8 compared the stress of steel fibers after elevated temperature, the maximum value among the legend represents the yield stress for steel fiber. The results indicate that the stress of steel fiber decreases gradually with the increasing temperature under the same strain rate. On one hand, this can be interpreted by the fact that the steel fiber can also be damaged when exposed to high temperature. On the other hand, the concrete crushing occurred before the steel fibers reached their full potential at high temperature mollification condition.

To quantitatively analyze the stress distribution of steel fibers within SFRC in different loading cases, the maximum and average stress as well as its standard deviation are summarized in Table 3. It can be found from Table 3 that the steel fiber stress distribution is uneven due to the random dispersion for fibers and heterogeneity of the microstructure of the concrete specimens, indicated by the great standard deviation. At each strain rate, both the maximum and average stress decreased as the experienced temperature increased. This is attributed to that the elevated temperature degrades the whole SFRC specimens, thus reducing the stress borne by steel fibers. Besides, in the cases with the same experienced temperature except for 800°C , the stress, especially the average stress, increases with an increasing strain rate. This can be explained by that when the strain rate is lower (i.e., $\dot{\epsilon} \leq 10 \text{ s}^{-1}$), most steel fibers have played a minor role because the stress is only dispersed to a few vertical fibers approximating to the loading direc-

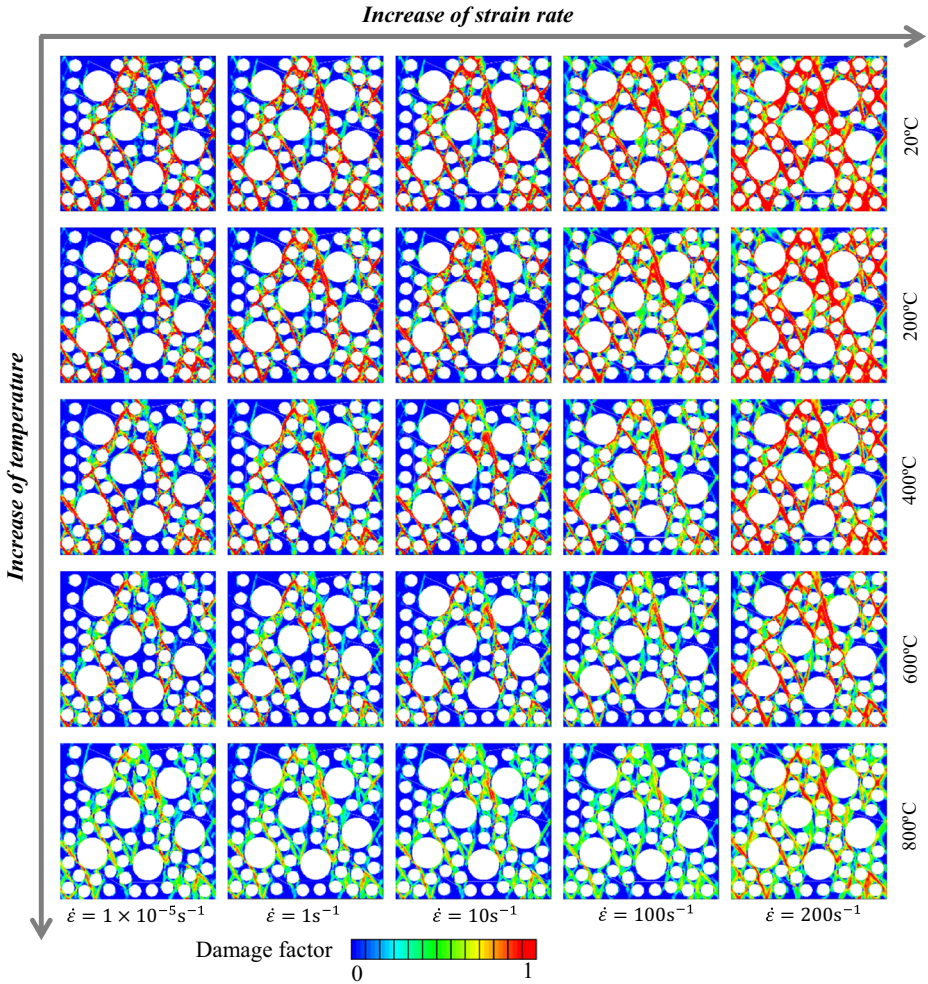


Figure 7. Compressive damage results of the SFRC under different strain rates at elevated temperature.

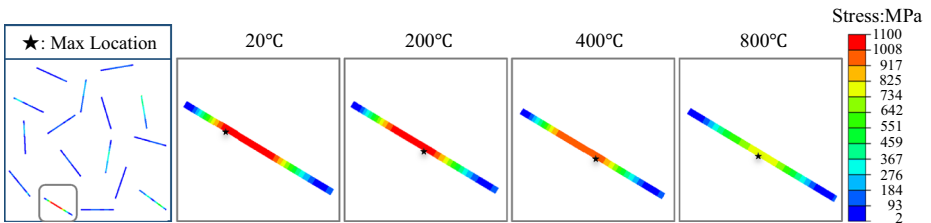


Figure 8. Comparison for steel fibers stress at elevated temperature.

Table 3
Stress Distribution of Steel Fibers (in MPa)

Strain rate (s^{-1})	20°C			200°C			400°C			600°C			800°C		
	Max.	Ava.	Std.	Max.	Ava.	Std.	Max.	Ava.	Std.	Max.	Ava.	Std.	Max.	Ava.	Std.
1×10^{-5}	1100	184	256	1000	174	237	1000	169	227	900	157	216	700	146	157
1	1100	180	256	1000	193	237	1000	164	232	900	171	213	700	113	170
10	1100	201	256	1050	204	245	1000	156	234	1000	196	243	700	168	170
100	1100	259	242	1100	334	229	1100	284	226	1000	273	224	400	164	92
200	1100	500	312	1100	488	280	1100	463	264	1100	348	281	1000	348	263

The maximum and average stress as well as its standard deviation are denoted as Max., Ava. and Std., respectively

tion. As the strain rate increases, more crack paths appear in the specimens, thus activating more fibers to resist cracking and more stress propagating to the fibers. Thence, improvement effect becomes more and more obvious under high strain rate. However, weak regularity exhibits for specimens after exposure to 800°C due to the severe temperature degradation. Nevertheless, it is acceptable that that steel fiber can commendably strengthen the dynamic impact performance of concrete materials.

3.3.3. Stress–Strain Relationship The dynamic compressive stress–strain curve of SFRC specimens under different strain rates are shown in Fig. 9. The stress–strain relationship flattens out significantly and the maximum stress decreases sharply with the increase of experienced temperature. This indicates that the high temperature also can distinctly degrade the mechanical properties of the fiber reinforced concrete, which is consistent with the results of Ren et al. [59]. Furthermore, it can be found that the SFRC still exist prominent strain rate effect according to transverse observation Fig. 9. Because inertia effect becomes more and more apparent under high strain rates (i.e. $\dot{\epsilon} \geq 100 \text{ s}^{-1}$), the peak stress and the corresponding strain were intensified dramatically. Jin et al. [60] illustrated that exter-

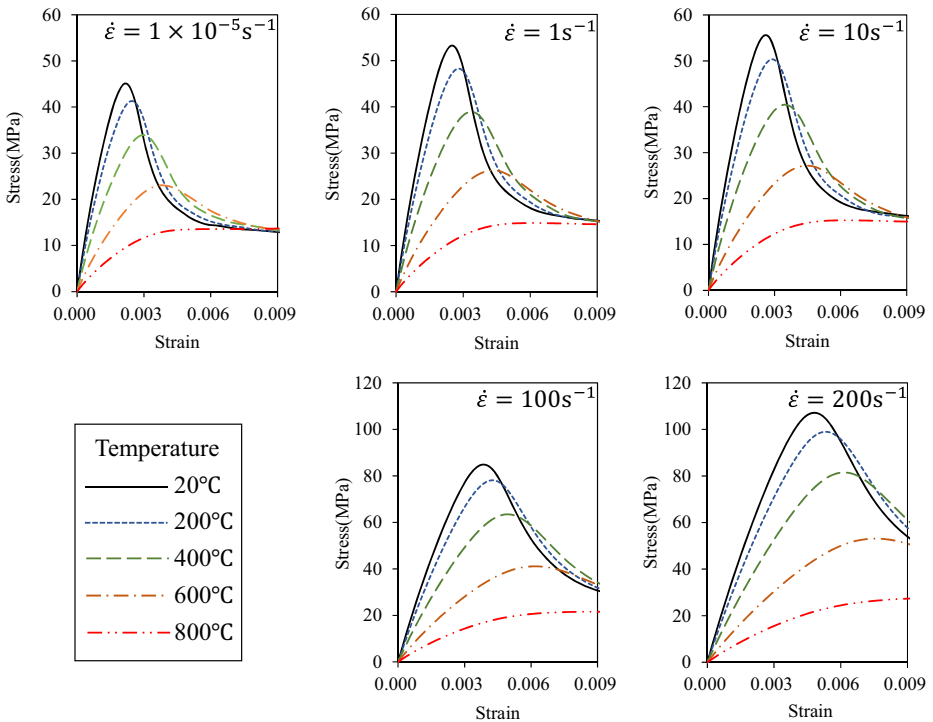


Figure 9. Stress–strain curves of the SFRC specimens under different strain rates.

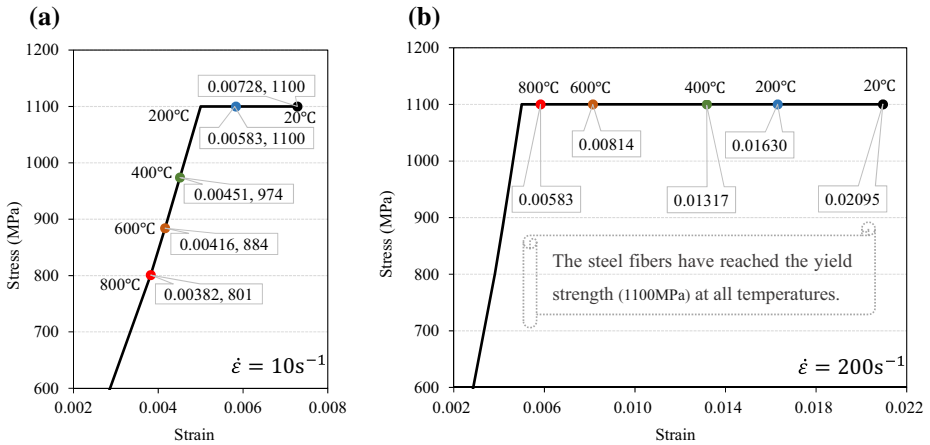


Figure 10. Stress-strain curves of steel fibers under different temperature. (a) Low strain rate ($\dot{\epsilon} = 10 \text{ s}^{-1}$); (b) high strain rate ($\dot{\epsilon} = 200 \text{ s}^{-1}$).

nal impulse or energy can only be offset by increasing the stress because of the short load action time of high-speed impact.

Figure 10a, b described the stress–strain curves of steel fibers under low strain rate and high strain rate after exposure to different temperature, respectively. One can discover that the steel fibers yield only in the cases high experienced temperature under low strain rate. Among them, the ultimate stress after high temperature is only 70–80% of the yield strength. On the contrary, the steel fibers have reached yield strength under high strain rate, regardless of experienced temperature. Furthermore, the ultimate strain of steel fibers at room temperature is approximately 2–3 times greater than that at high temperature (600–800°C). Combined with stress distribution of steel fibers in Fig. 8 and Table 3, it is obvious that steel fibers have play more important role under high strain rate. In addition, it must be mentioned that the ultimate damage depends on the sharply decreasing strength of concrete because of high temperature degeneration effect, which explains the reason why the ultimate strain of steel fiber decreases with the increasing experienced temperature.

3.3.4. Dynamic Compressive Increase Factor (CDIF) The dynamic compressive strength increase factor (CDIF) is used to describe the phenomenon that the strength of materials increases with the strain rate increasing, which can be calculated by the ratio of dynamic compressive strength to the quasi-static compressive strength (i.e., $\dot{\epsilon} = 1 \times 10^{-5} \text{ s}^{-1}$ in the present study). Figure 11 presents the scatter relationship between the obtained CDIF and strain rate at room temperature ($T = 20^\circ\text{C}$) and high temperature ($T = 800^\circ\text{C}$). Meanwhile, the exact CDIF values of SFRC and PC after elevated temperature are shown in Table 4. It can be found that the SFRC also exhibit obvious strain rate effect, irrespective of experienced temperature. Nonetheless, the CDIF after high temperature is inferior to

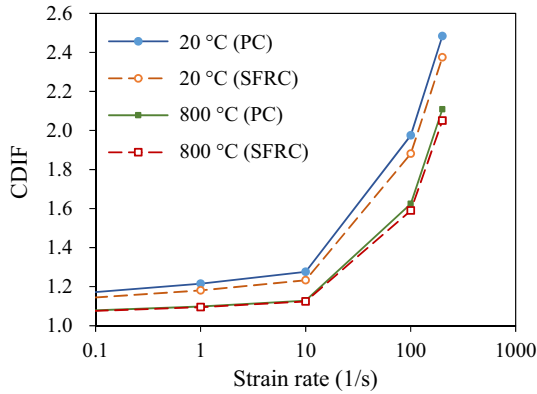


Figure 11. Relationship between CDIF and strain rate at room and high temperature.

Table 4 CDIF Under Different Strain Rates at Elevated Temperature

Temperature (°C)	Material	CDIF at various strain rates			
		1 s ⁻¹	10 s ⁻¹	100 s ⁻¹	200 s ⁻¹
20	PC	1.215	1.276	1.975	2.484
	SFRC	1.181	1.233	1.881	2.375
400	PC	1.159	1.210	2.015	2.600
	SFRC	1.148	1.193	1.872	2.404
800	PC	1.098	1.128	1.624	2.108
	SFRC	1.095	1.124	1.590	2.050

PC plain concrete, SFRC steel fiber reinforced concrete

that at room temperature, this can be construed that the lateral inertia effect of concrete material is weakened due to structure loosening after elevated temperature. Meanwhile, similar to plain concrete, it also demonstrates that the compressive strength of SFRC is more dramatically affected by the temperature degradation effect compared with the strain rate effect. Besides, the strain rate sensitivity of SFRC is clearly lower than that of plain concrete.

3.3.5. Steel Fiber Enhancement Effect The fiber reinforcement degree of compressive strength is described by steel fiber enhancement factor, which is the ratio of compressive strength of SFRC and that of plain concrete. Table 5 shows the steel fiber enhancement factor of compressive strength under different strain rates after elevated temperature. Meanwhile, the relationship between steel fiber reinforcement effect and temperature as well as strain rate are presented in Fig. 12. It is not difficult to find that the fiber enhancement effect is weakened with increasing the strain rate. For one thing, the action of steel fiber is affected by crushed con-

Table 5
Steel Fiber Enhancement Factor of Compressive Strength

Temperature (°C)	Steel fiber enhancement factor at different strain rates				
	$1 \times 10^{-5} \text{ s}^{-1}$	1 s^{-1}	10 s^{-1}	100 s^{-1}	200 s^{-1}
20	1.090	1.059	1.053	1.038	1.042
200	1.112	1.084	1.075	1.045	1.044
400	1.144	1.134	1.128	1.064	1.058
600	1.195	1.189	1.185	1.126	1.101
800	1.237	1.233	1.231	1.211	1.203

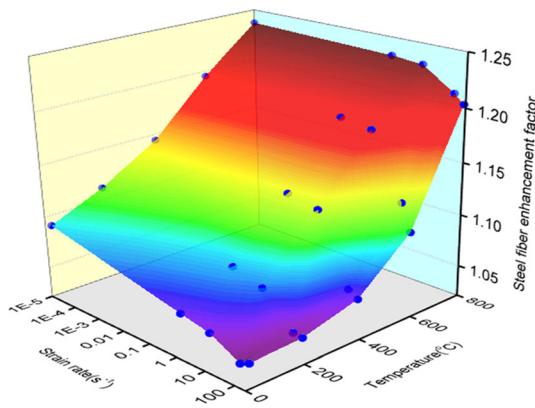


Figure 12. Steel fiber reinforcement effect at different strain rates at room and elevated temperature.

crete under fast impact speed; for another thing, the steel fiber enhancement factor just expresses the potentiation of strength and not involves the reinforcement of failures mode. One can discover that the fiber improvement effect in failure patterns becomes more and more obvious with the increase of strain rate from the analysis in Sect. 3.3.1. A possible explanation for this observation is that at high strain rates, the number of crack path within the specimens becomes larger, compared with that in a quasi-static case. Thus, more fibers are activated to resist cracking, resulting in less scatters of the specimen. Nevertheless, specimens with less cracks absorb less energy, exhibiting a weaker increase in strength.

Furthermore, it also can be found that the fiber enhancement effect is more significant with the increasing temperature. As previously mentioned, this is because good thermal conduction property of steel fiber can reduce temperature-induced damage within the SFRC specimens. Meanwhile, the greater dilatancy of concrete after high temperature can activate more fibers to play their confinement roles. The steel fiber has high(er) strength and large(r) crack resistance, whose function in heterogeneous concrete becomes more remarkable as the increase of temperature. In other words, the steel fibers improvement effect of the mechanical proper-

ties of concrete after exposure to elevated temperature is more distinct than that at room temperature.

4. Conclusive Remarks

Based on the mesoscopic numerical simulation method, the dynamic behavior of SFRC with different fiber lengths after elevated temperatures was compared. The stress distributions of steel fibers under different strain rate were discussed, and the influences of experienced temperature and strain rate on the steel fiber enhancement effect were analyzed. According to the simulation results, some conclusions can be drawn below.

1. The steel fiber can effectively improve the dynamic mechanical properties of concrete materials after high temperature because of its good transverse bonding effect and thermal conduction property.
2. The stress is concentrated on the periphery of vertical fibers whose direction is similar to the loading. The steel fibers can more adequately prevent crack evolution under high strain rate after high temperature.
3. Under low strain rate, the ultimate stress of steel fibers after high temperature is only 70–80% of the yield strength. The ultimate strain at room temperature is approximately 2–3 times greater than that after high temperature.
4. The fiber enhancement effect on strength is weakened with the increasing strain rate, while that is more significant with the increase of experienced temperature.

In present study, the fiber shape and the bond-slip interaction between fibers and mortar matrix are not considered tentatively, which will be an important direction of the subsequent research on SFRC. Moreover, a series of experimental test is in need to further calibrated the proposed numerical approach for SFRC in a complicated loading scenario.

Funding

Funding was provided by National Natural Science Foundation of China (Grant Nos. 51822801 and 51978022).

References

1. Hao H, Hao Y, Li J, Chen W (2016) Review of the current practices in blast-resistant analysis and design of concrete structures. *Adv Struct Eng* 19(8):1193–1223
2. Huo JS, He YM, Xiao LP, Chen BS (2013) Experimental study on dynamic behaviours of concrete after exposure to high temperatures up to 700°C. *Mater Struct* 46(1/2):255–265

3. Chen L, Fang Q, Jiang X, Ruan Z, Hong J (2015) Combined effects of high temperature and high strain rate on normal weight concrete. *Int J Impact Eng* 86:40–56
4. Park S, Yim HJ (2016) Evaluation of residual mechanical properties of concrete after exposure to high temperatures using impact resonance method. *Constr Build Mater* 129:89–97
5. Ma Q, Guo R, Zhao Z, Lin Z, He K (2015) Mechanical properties of concrete at high temperature—a review. *Constr Build Mater* 93:371–383
6. Malvar LJ, Ross CA (1998) Review of strain rate effects for concrete in tension. *ACI Mater J* 95(6):735–739
7. Zende A, Kulkarni A, Hutagi A (2013) Behavior of reinforced concrete subjected to high temperatures—a review. *J Struct Fire Eng* 4(4):281–295
8. Bischoff PH, Perry SH (1991) Compressive behaviour of concrete at high strain rates. *Mater Struct* 24(6):425–450
9. Thomas RJ, Sorensen AD (2017) Review of strain rate effects for UHPC in tension. *Constr Build Mater* 153:846–856
10. European Committee for Standardization (2004) Eurocode 2: design of concrete structures—part 1–2: general rules-structural fire design, EN 1992-1-2:2004. The Committee, Brussels
11. Marcos-Meson V, Michel A, Solgaard A, Fischer G, Edvardsen C, Skovhus TL (2018) Corrosion resistance of steel fibre reinforced concrete—a literature review. *Cem Concr Res* 103:1–20
12. Lok TS, Zhao PJ (2004) Impact response of steel fiber-reinforced concrete using a split Hopkinson pressure bar. *ASCE J Mater Civil Eng* 16(1):54–59
13. Lau A, Anson M (2006) Effect of high temperatures on high performance steel fibre reinforced concrete. *Cem Concr Res* 36(9):1698–1707
14. Wang Z, Liu Y, Shen RF (2008) Stress–strain relationship of steel fiber-reinforced concrete under dynamic compression. *Constr Build Mater* 22(5):811–819
15. Wang ZL, Shi ZM, Wang JG (2011) On the strength and toughness properties of SFRC under static–dynamic compression. *Compos Part B-Eng* 42(5):1285–1290
16. Liang X, Wu C (2018) Meso-scale modelling of steel fibre reinforced concrete with high strength. *Constr Build Mater* 165:187–198
17. Dügenci O, Haktanir T, Altun F (2015) Experimental research for the effect of high temperature on the mechanical properties of steel fiber-reinforced concrete. *Constr Build Mater* 75:82–88
18. Sun X, Zhao K, Li Y, Huang R, Ye Z, Zhang Y, Ma J (2018) A study of strain-rate effect and fiber reinforcement effect on dynamic behavior of steel fiber-reinforced concrete. *Constr Build Mater* 158:657–669
19. Yoo D, Banthia N (2017) Mechanical and structural behaviors of ultra-high-performance fiber-reinforced concrete subjected to impact and blast. *Constr Build Mater* 149:416–431
20. Caverzan A, Cadoni E, di Prisco M (2013) Dynamic tensile behaviour of high performance fibre reinforced cementitious composites after high temperature exposure. *Mech Mater* 59:87–109
21. Xiao J, Li Z, Xie Q, Shen L (2016) Effect of strain rate on compressive behaviour of high-strength concrete after exposure to elevated temperatures. *Fire Saf J* 83:25–37
22. Zhai C, Chen L, Fang Q, Chen W, Jiang X (2017) Experimental study of strain rate effects on normal weight concrete after exposure to elevated temperature. *Mater Struct* 50(1):40
23. Yao W, Liu H, Xu Y, Xia K, Zhu J (2017) Thermal degradation of dynamic compressive strength for two mortars. *Constr Build Mater* 136:139–152

24. Jin L, Hao H, Zhang R, Du X (2018) Determination of the effect of elevated temperatures on dynamic compressive properties of heterogeneous concrete: a meso-scale numerical study. *Constr Build Mater* 188:685–694
25. Dassault Systèmes Simulia (2014) ABAQUS 6.14
26. Wriggers P, Moftah SO (2006) Mesoscale models for concrete: homogenisation and damage behaviour. *Finite Elem Anal Des* 42(7):623–636
27. Shadafza E, Saleh Jalali R (2016) The elastic modulus of steel fiber reinforced concrete (SFRC) with random distribution of aggregate and fiber. *Civil Eng Infrastruct J* 49:21–32
28. Pedersen RR, Simone A, Sluys LJ (2013) Mesoscopic modeling and simulation of the dynamic tensile behavior of concrete. *Cem Concr Res* 50:74–87
29. Du X, Jin L, Ma G (2014) A meso-scale numerical method for the simulation of chloride diffusivity in concrete. *Finite Elem Anal Des* 85:87–100
30. Jin L, Zhang R, Du X (2018) Characterisation of the temperature-dependent heat conduction in heterogeneous concretes. *Mag Concr Res* 70:325–339
31. Grondin F, Matallah M (2014) How to consider the interfacial transition zones in the finite element modelling of concrete?. *Cem Concr Res* 58:67–75
32. Šavija B, Pacheco J, Schlangen E (2013) Lattice modeling of chloride diffusion in sound and cracked concrete. *Cem Concr Compos* 42:30–40
33. Šavija B, Luković M, Pacheco J, Schlangen E (2013) Cracking of the concrete cover due to reinforcement corrosion: a two-dimensional lattice model study. *Constr Build Mater* 44:626–638
34. Du X, Jin L (2014) Meso-scale numerical investigation on cracking of cover concrete induced by corrosion of reinforcing steel. *Eng Fail Anal* 39:21–33
35. Xu Z, Hao H, Li HN (2012) Mesoscale modelling of fibre reinforced concrete material under compressive impact loading. *Constr Build Mater* 26(1):274–288
36. Fang Q, Zhang J (2013) Three-dimensional modelling of steel fiber reinforced concrete material under intense dynamic loading. *Constr Build Mater* 44:118–132
37. Xu Z, Hao H, Li HN (2012) Mesoscale modelling of dynamic tensile behaviour of fibre reinforced concrete with spiral fibres. *Cem Concr Res* 42(11):1475–1493
38. Crank J, Nicolson P (1996) A practical method for numerical evaluation of solutions of partial differential equations of the heat-conduction type. *Adv Comput Math* 6(1):207–226
39. Zoth G, Hänel R (1988) Appendix. In: Haenel R, Rybach L, Stegena L (eds) *Handbook of terrestrial heat-flow density determination* Kluwer Academic Publishers, Dordrecht, pp 449–468
40. Černý R, Maděra J, Poděbradská J, Toman J, Drchalová J, Klečka T, Jurek K, Rovnaníková P (2000) The effect of compressive stress on thermal and hygric properties of Portland cement mortar in wide temperature and moisture ranges. *Cem Concr Res* 30(8):1267–1276
41. Vosteen H, Schellschmidt R (2003) Influence of temperature on thermal conductivity, thermal capacity and thermal diffusivity for different types of rock. *Phys Chem Earth (Parts A/B/C)* 28(9/11):499–509
42. Grassl P, Pearce C (2010) Mesoscale approach to modeling concrete subjected to thermomechanical loading. *ASCE J Eng Mech* 136(3):322–328
43. CEB-FIP (2010) CEB-FIP model code 2010, fib Bulletin 55. International Federation for Structural Concrete, Lausanne, Switzerland
44. China Association for Engineering Construction Standardization (2006) Technical code for fire safety of steel structure in buildings, CECS 200: 2006. China Planning Press, Beijing

45. Khan MI (2002) Factors affecting the thermal properties of concrete and applicability of its prediction models. *Build Environ* 37(6):607–614
46. Huan Y, Fang Q, Chen L, Zhang Y (2008) Evaluation of blast-resistant performance predicted by damaged plasticity model for concrete. *Trans Tianjin Univ* 14:414–421
47. Aref AJ, Dolatshahi KM (2013) A three-dimensional cyclic meso-scale numerical procedure for simulation of unreinforced masonry structures. *Comput Struct* 120:9–23
48. Du X, Jin L, Ma G (2014) Numerical simulation of dynamic tensile-failure of concrete at meso-scale. *Int J Impact Eng* 66:5–17
49. Lubliner J, Ollivier J, Oller S, Oñate E (1989) A plastic-damage model for concrete. *Int J Solids Struct* 25(3):299–326
50. Lee J, Fenves G (1998) Plastic-damage model for cyclic loading of concrete structures. *ASCE J Eng Mech* 124(8):892–900
51. Zhai C, Chen L, Xiang H, Fang Q (2016) Experimental and numerical investigation into RC beams subjected to blast after exposure to fire. *Int J Impact Eng* 97:29–45
52. Qiu Y, Lin Z (2006) Testing study on damage of granite samples after high temperature. *Rock Soil Mech* 27(6):1005–1010(in Chinese)
53. Chen Y, Ni J, Shao W, Azzam R (2012) Experimental study on the influence of temperature on the mechanical properties of granite under uni-axial compression and fatigue loading. *Int J Rock Mech Min* 56:62–66
54. Comité Euro-International du Béton (1988) Concrete structures under impact and impulsive loading, CEB Bulletin No. 187. The Committee, Lausanne, Switzerland
55. ISO (1999) Fire resistance test on elements of building construction, ISO 834-1. International Standards Organization, Geneva
56. Gao C (2013) Experimental research on mechanical properties of concrete and reinforced concrete after high temperature. Yangzhou University, Yangzhou(in Chinese)
57. Bamonte P, Gambarova PG (2010) Thermal and mechanical properties at high temperature of a very high-strength durable concrete. *ASCE J Mater Civil Eng* 22(6):545–555
58. Ripani M, Etse G, Vrech S, Mroginski J (2014) Thermodynamic gradient-based poro-plastic theory for concrete under high temperatures. *Int J Plast* 61:157–177
59. Ren W, Xu J, Su H (2016) Dynamic compressive behavior of basalt fiber reinforced concrete after exposure to elevated temperatures. *Fire Mater* 40(5):738–755
60. Jin F, Xu J, Fan F, Su H (2013) Strength property of steel fiber reinforced concrete at elevated temperature. *B Chin Ceram Soc* 32(4):683–686(in Chinese)